Euler Flutter Analysis of Airfoils Using Unstructured Dynamic Meshes

Russ D. Rausch*
Purdue University, West Lafayette, Indiana 47907
John T. Batina†
NASA Langley Research Center, Hampton, Virginia 23665-5225
and
Henry T. Y. Yang‡
Purdue University, West Lafayette, Indiana 47907

Modifications to a two-dimensional, unsteady Euler code for the aeroelastic analysis of airfoils are described. The modifications involve including the structural equations of motion and their simultaneous time integration with the governing flow equations. A novel aspect of the capability is that the solutions are obtained using unstructured grids made up of triangles. Comparisons are made with parallel calculations performed using linear theory and a structured grid Euler code to assess the accuracy of the unstructured grid Euler results. Results are presented for a flat-plate airfoil and the NACA 0012 airfoil to demonstrate applications of the Euler code for generalized force computations and aeroelastic analysis. In these comparisons, two different finite-volume discretizations of the Euler equations on unstructured meshes were employed. Sensitivity of the Euler results to changes in numerical parameters was also investigated.

Nomenclature

A_{ij} = generalized aerodynamic force resulting from pressure induced by mode j acting through mode i
a = nondimensional distance from midchord to elastic axis
a_∞ = freestream speed of sound
b = airfoil semichord, $c/2$
C_p = pressure coefficient
c = airfoil chord
c_i = generalized damping of mode i
k = reduced frequency, $\omega c/2U_\infty$
k_i = generalized frequency of mode i
M_∞ = freestream Mach number
m = airfoil mass per unit span
m_i = generalized mass of mode i
$\bar{Q}$ = nondimensional dynamic pressure $[U_\infty/(b\omega_\alpha\sqrt{\mu})]^2$
$\bar{Q}_f$ = nondimensional dynamic pressure at flutter
Q_i = generalized force in mode i
q_i = generalized displacement of mode i
r_α = airfoil radius of gyration about elastic axis
s = Laplace transform variable, $\sigma + i\omega$
T = time, s
t = time, nondimensionalized by freestream speed of sound and airfoil chord, Ta_∞/c
U_∞ = streamwise freestream speed
u_i = load vector
x_i = state vector
x_α = nondimensional distance from elastic axis to mass center
α_0 = mean angle of attack
$\Delta\tilde{C}_p$ = unsteady lifting pressure coefficient normalized by the amplitude of oscillation
Θ = integral of state-transition matrix
μ = airfoil mass ratio, $m/\pi\rho_\infty b^2$
ρ_∞ = freestream density
σ = real part of Laplace transform variable
Φ = state-transition matrix
ω = angular frequency
ω_h = uncoupled natural frequency of bending mode
ω_α = uncoupled natural frequency of torsion mode

Introduction

CONSIDERABLE progress has been made over the past decade on developing computer codes for transonic aeroelastic analysis.[1] This research has been highly focused on developing finite-difference codes for the solution of the transonic small-disturbance[2,3] and full-potential[4,5] equations, although efforts are currently underway at the higher equation levels as well.[6-10] The above work on aeroelastic analysis with the Euler and Navier-Stokes equations has all been done with flow solvers that assume that the computational grid has an underlying geometrical structure. The applications have also been limited to simple geometries such as airfoils and wings. Several problems arise, however, in extending these procedures to treat more complicated geometries. For example, it is generally recognized that it is difficult to generate a structured grid about a complete aircraft configuration. Other difficulties arise in moving the grid for aeroelastic motion where the grid must conform to the instantaneous shape of the vehicle. Therefore, an alternative approach that can treat complex aircraft configurations undergoing realistic deformations and motions is desired.

An alternative approach for the modeling of complex aircraft configurations is the use of unstructured meshes.[11-14] In two dimensions these meshes are constructed from triangles

Received Feb. 19, 1989; presented as Paper 89-1384 at the 30th Structures, Structural Dynamics, and Materials Conference, Mobile, AL, April 3-5, 1989.

*Graduate Research Assistant, School of Aeronautics and Astronautics. Member AIAA.
†Senior Research Scientist, Unsteady Aerodynamics Branch, Structural Dynamics Division. Senior Member AIAA.
‡Professor and Dean, Schools of Engineering. Fellow AIAA.

and in three dimensions they consist of an assemblage of tetrahedra. These triangles or tetrahedra are oriented to conform to the geometry being considered, thus making possible the treatment of complicated shapes. Applications of these methods have been demonstrated for multielement airfoils[11,12] and complete aircraft configurations.[13,14] A further advantage of the unstructured grid methods is that they easily permit mesh refinement in regions of high-flow gradients to more accurately resolve the physics of the flow.[12,15,16]

An assessment of the applicability of the unstructured grid methodology for unsteady aerodynamic analysis of airfoils was reported in Ref. 17 where an unsteady Euler solver based on an unstructured grid of triangles was developed to treat oscillating airfoils. The capability included a dynamic mesh algorithm to allow for airfoil motion. The algorithm is quite general in that it can treat realistic motions and deformations of multiple two-dimensional bodies.

The purpose of this study was to extend the two-dimensional, unsteady Euler code of Ref. 17 to the aeroelastic analysis of airfoils. This represents a first step toward aeroelastic analysis of aircraft using unstructured meshes.[18] Results are presented for a flat-plate airfoil and for the NACA 0012 airfoil to demonstrate applications of the Euler code to generalized aerodynamic force computation and aeroelastic analysis. Detailed comparisons are made for results obtained using the two-dimensional Euler code, the CFL3D[19] Euler/Navier-Stokes code, and linear theory.[20] These comparisons permit an assessment of the accuracy of the Euler code for such applications. In these comparisons, two different finite-volume discretizations of the Euler equations on unstructured meshes are employed. Sensitivity of the Euler results to changes in numerical parameters was also investigated.

Euler Solution Algorithm

The two-dimensional, unsteady Euler equations are solved using the multistage Runge-Kutta, time-stepping scheme of Ref. 17. This algorithm uses a finite-volume spatial discretization for solution on an unstructured grid made up of triangles. The original algorithm of Ref. 17 was a node-based scheme whereby the flow variables are stored at the vertices of the triangles. A second algorithm, a cell-centered scheme, was also employed in the present study. This second scheme is based on unpublished work of the second author. In the cell-centered scheme, the flow variables are stored at the centroids of the triangles. In both algorithms, artificial dissipation is added explicitly to prevent oscillations near shock waves and to damp high-frequency uncoupled error modes. Specifically, an adaptive blend of harmonic and biharmonic operators is used, corresponding to second- and fourth-difference dissipation, respectively. The biharmonic operator provides a background dissipation to damp high frequency errors, and the harmonic operator prevents oscillations near shock waves. The algorithms also employ enthalpy damping, local time stepping, and implicit residual smoothing to accelerate convergence to steady state. The local time stepping uses the maximum allowable step size at each grid point for the node-based scheme and for each triangle in the cell-centered scheme, as determined by a local stability analysis. The implicit residual smoothing permits the use of local time steps that are larger than those imposed by the Courant-Fredricks-Lewy stability condition. This is achieved by averaging the residuals implicitly with neighboring values. A time-accurate version of the residual smoothing is also used for global time stepping during unsteady applications of the code.

With respect to boundary conditions, a characteristic analysis based on Riemann invariants is used to determine the values of the flow variables on the outer boundary of the grid. This analysis correctly accounts for wave propagation in the farfield, which is important for rapid convergence to steady state and serves as a nonreflecting boundary condition for unsteady applications.

Dynamic Mesh Algorithm

A dynamic mesh algorithm is used to move the mesh for unsteady airfoil calculations. The method, as developed in Ref. 17, models the triangulated mesh as a spring network where each edge of each triangle represents a spring with stiffness inversely proportional to the length of that edge. In this procedure, grid points along the outer boundary of the mesh are held fixed, and the instantaneous locations of the points on the airfoil (inner boundary) are specified. For aeroelastic calculations, the position of the inner boundary is determined by the structural equations of motion. The locations of the interior nodes are then determined by solving the static equilibrium equations that result from a summation of forces at each node in both the x and y directions. The solution of the equilibrium equations is approximated by using a predictor-corrector procedure, which first predicts the new locations of the nodes by extrapolation from grids at previous time levels and then corrects these locations by using several Jacobi iterations of the static equilibrium equations. The predictor-corrector procedure is relatively efficient because only one or two Jacobi iterations are required to move the mesh accurately.

Pulse Transfer Function Analysis

Generalized aerodynamic forces, which are typically used in aeroelastic analyses, may be obtained by calculating several cycles of a harmonically forced oscillation with the determination of the forces based on the last cycle of oscillation. The method of harmonic oscillation requires one calculation for each value of reduced frequency of interest. By contrast, generalized forces may be determined for a wide range of reduced frequency in a single calculation by the pulse transfer function analysis.[21,22] This, of course, relies on the local linearity of the airloads with respect to mode and amplitude of motion, which must be assured for reliable use of the method.

Time-Marching Aeroelastic Analysis

In this section the aeroelastic equations of motion, the time-marching solution procedure, and the modal identification technique are described.

Aeroelastic Equations of Motion

The aeroelastic equations of motion can be written for each mode i as

$$m_i\ddot{q}_i + c_i\dot{q}_i + k_iq_i = Q_i \tag{1}$$

where q_i is the generalized normal mode displacement, m_i is the generalized mass, c_i is the generalized damping, k_i is the generalized stiffness, and Q_i is the generalized force computed by integrating the pressure weighted by the mode shapes. These equations of motion are derived by assuming that the deformation of the body under consideration can be described by a separation of variables involving the summation of free vibration modes weighted by generalized displacements. This analysis differs from the traditional form of the two-dimensional aeroelastic equations of motion, which are usually written in terms of plunge and pitch degrees of freedom. This normal mode form of the equations was implemented in the present study due to the relative ease of extending the methodology to three-dimensional structures where the normal mode representation is most common.

Time-Marching Solution

The solution procedure for integrating Eq. (1) is similar to that described by Edwards et al.[23,24] A similar formulation is implemented in the present study for multiple degrees of freedom. Here the linear state equations are written as

$$\dot{x}_i = Ax_i + Bu_i \tag{2}$$

where A and B are coefficient matrices that result from the change of variables $x_i = [q_i\ \dot{q}_i]^T$, and u_i is the nondimensional

generalized force weighted by mode i. Equation (2) is integrated in time using the modified state-transition matrix structural integrator[24] implemented as a predictor-corrector procedure according to

Predictor:

$$x_i^{n+1} = \Phi x_i^n + \Theta B(3u_i^n - u_i^{n-1})/2 \tag{3a}$$

Corrector:

$$x_i^{n+1} = \Phi x_i^n + \Theta B(u_i^{n+1} + u_i^n)/2 \tag{3b}$$

where Φ is the state-transition matrix, and Θ the integral of the state-transition matrix from time step n to $n+1$.

Modal Identification Technique

Damping and frequency characteristics of the aeroelastic responses are estimated from the response curves by using the modal identification technique of Bennett and Desmarais.[25] The modal estimates are determined by a least-squares curve fit of the responses of the form

$$q_i(T) = a_0 + \sum_{j=1}^{m} e^{\sigma_j T}[a_j \cos(\omega_j T) + b_j \sin(\omega_j T)], \quad i = 1,2 \tag{4}$$

where m is the number of modes which was selected to be equal to two in the present study.

State-Space Aeroelastic Stability Analysis

As an alternative to the time-marching analysis, aeroelastic stability analyses were performed using state-space aeroelastic modeling as developed in Refs. 26 and 27. This locally linear aeroelastic stability analysis is relatively inexpensive and retains the nonlinear properties of the transonic mean flow. The model is derived by curve fitting the generalized force transfer functions obtained from transient responses resulting from pulsed motions of the airfoil modes. These Padé approximating functions[26] may be written as a set of ordinary differential equations and coupled to the airfoil equations of motion. This leads to a linear first-order matrix equation, which can be solved using linear eigenvalue solution techniques. The resulting eigenvalues are plotted in a dynamic pressure root-locus type format in the complex s plane.

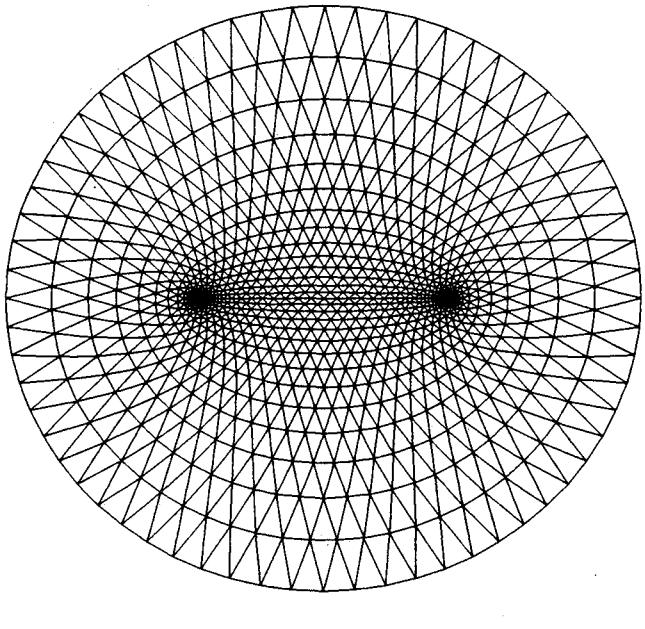

Fig. 1 Partial view of 64 × 32 grid of triangles about the flat-plate airfoil.

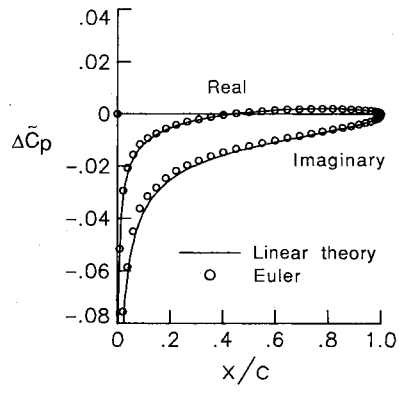

a) plunge motion

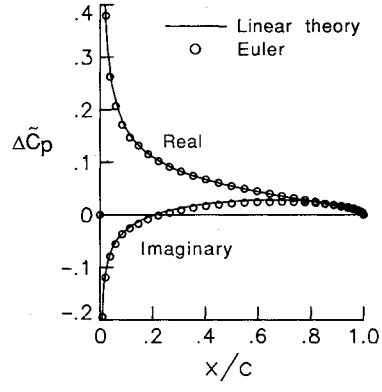

b) pitch motion

Fig. 2 Comparisons of unsteady pressure distributions computed using linear theory and the node-based Euler algorithm for the flat-plate airfoil undergoing harmonic motion at $M_\infty = 0.5$, $\alpha_0 = 0$ deg, and $k = 0.25$.

Results and Discussion

To assess the accuracy of the two-dimensional, unstructured grid Euler code for generalized force computation and aeroelastic analysis, calculations were performed for a flat-plate airfoil and for the NACA 0012 airfoil. Comparisons are made with parallel calculations performed using alternative methods. Generalized aerodynamic forces were computed using the pulse transfer-function analysis as well as by simple harmonic oscillation for several values of reduced frequency. In the harmonic calculations, the airfoil was forced to oscillate for three cycles to obtain a periodic solution using 2500 steps/cycle of motion. Both plunge and pitch-about-the-quarter-chord motions were considered. The amplitudes of oscillation were 0.01 chord lengths and 0.1 deg for plunge and pitch, respectively. Aeroelastic results are presented for a much studied configuration designated as case A in Ref. 28, which has normal modes similar to those of a streamwise section near the tip of a swept-back wing. The wind-off bending and torsion frequencies are 71.33 and 535.65 rad/s, respectively. The pivot point for the bending mode is located 1.44 chord lengths upstream of the leading edge of the airfoil. The pivot point for the torsion mode is 0.068 chord lengths forward of midchord. These mode shapes and natural frequencies were determined by performing a free vibration analysis with the aeroelastic equations of motion written in the traditional form using the following structural parameter values: $a = -2.0$, $x_\alpha = 1.8$, $r_\alpha = 1.865$, $\omega_h = 100$ rad/s, and $\omega_\alpha = 100$ rad/s. Also, the airfoil mass ratio was $\mu = 60$. Generalized displacements corresponding to the inertially coupled modes are defined as q_1 and q_2, respectively. Initial conditions for the time-marching aeroelastic analysis were $\dot{q}_1(0) = 2$ and $\dot{q}_2(0) = 0.01$.

Flat-Plate Airfoil Results

Calculations were performed for a flat-plate airfoil to assess the accuracy of the unstructured grid Euler code for a simple configuration where a highly accurate linear theory solution is available for comparison. The results were obtained using a mesh of triangles, which was generated analytically by a modified Joukowski transformation. A partial view of the mesh is shown in Fig. 1. The grid has 2048 nodes, 4096 triangles, and extends 20 chord lengths from the airfoil with a circular outer boundary. Also, there are 64 points which lie on the surface of the airfoil. Calculations were performed for the flat-plate airfoil at a freestream Mach number of $M_\infty = 0.5$ and 0 deg angle of attack. Results were obtained using both the node-based and the cell-centered spatial discretizations of the Euler equations. Comparisons are made with computations performed using the linear theory program of Ref. 20, which is based on the kernel-function method.

Unsteady Pressure Comparisons

Unsteady pressure distributions due to simple harmonic motion were computed for the flat-plate airfoil to determine the accuracy of the pressures by making comparisons with linear theory results. The Euler results shown were obtained using the node-based discretization of the Euler equations. The calculations were performed at a reduced frequency based on semichord of $k = 0.25$ for both plunge and pitch-about-the-quarter-chord motions. These results are presented in Fig. 2 as real and imaginary components of the lifting pressure coefficient normalized by the amplitude of oscillation $\Delta\tilde{C}_p$. The comparisons between Euler and linear theory pressure distributions indicate good agreement between the two sets of results, which tend to verify the Euler calculations. In these comparisons the real parts of the pressure distributions agree slightly better than the imaginary parts. Also, the largest differences occur in the imaginary part of the unsteady pressure due to plunge (Fig. 2a) which is underpredicted in comparison with linear theory. Furthermore, a fundamental difference between the Euler and linear theory pressure distributions is the fact that the pressure jump at the leading edge is zero in the Euler calculation with the node-based scheme in comparison with infinity predicted by linear theory. The Euler pressure jump is zero at the leading edge since the grid point here can be defined as either an upper surface or lower surface point and hence $\Delta\tilde{C}_p = 0$. According to linear theory, however, there is a square-root singularity in the lifting pressure coefficient at the leading edge. Consequently, some of the differences in the Euler pressures on the surface of the airfoil aft of the leading edge and subsequent differences in generalized forces in comparison with linear theory may be attributed to this fundamental difference in the character of the solutions near the leading edge.

Generalized Force Comparisons

Generalized aerodynamic forces for the flat-plate airfoil are presented in Fig. 3; they are computed using three different methods including the pulse analysis, the harmonic analysis, and linear theory. Here, both sets of Euler results were first obtained using the node-based spatial discretization of the Euler equations. The results are plotted as real and imaginary components of the unsteady forces A_{ij} as a function of reduced frequency k. In this section, plunge and pitch-about-the-quarter-chord are defined as modes 1 and 2, respectively. Thus, for example, A_{12} is the lift coefficient due to pitching. The harmonic results were obtained at five values of reduced frequency: $k = 0.0, 0.25, 0.50, 0.75$, and 1.0. These results are used to determine the accuracy of the results obtained using the pulse analysis. Both of these sets of results are compared with linear theory results, which are the correct solution for this case.

As should be expected, the Euler forces computed using the pulse analysis are in excellent agreement with the forces computed using simple harmonic motion at all values of reduced frequency that were considered. Both of these sets of forces agree reasonably well with the linear theory forces at the lower values of reduced frequency, although differences occur at the higher values of reduced frequency. For example, for the lift coefficient due to plunge A_{11}, the imaginary part is underpredicted by approximately 20% at $k = 1.0$ in comparison with linear theory. Also, the forces due to pitch compare slightly better than the forces due to plunge.

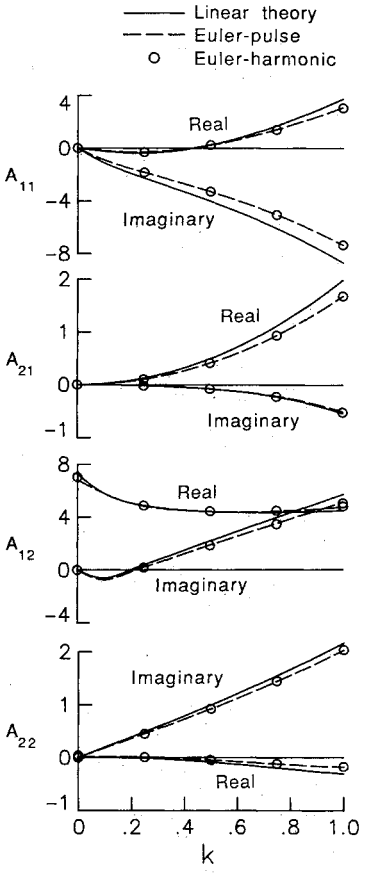

Fig. 3 Comparisons of generalized aerodynamic forces computed using linear theory and the node-based Euler algorithm for the flat-plate airfoil at $M_\infty = 0.5$ and $\alpha_0 = 0$ deg.

To investigate the source of the discrepancies between Euler and linear theory forces, many numerical parameters in the node-based algorithm were varied. These variations include: 1) mesh refinement, 2) the amplitude of motion, 3) how many Jacobi iterations were used in the dynamic mesh capability, 4) whether the mesh was moved rigidly following the airfoil motion or with the dynamic mesh capability, 5) the temporal order of accuracy in the numerical determination of grid speeds, 6) whether the grid speeds were determined numerically or analytically, 7) the level of explicit artificial dissipation that was used in the calculation, and 8) whether or not implicit residual smoothing was used to increase the allowable step size. In all cases, the results compared to plotting accuracy and are thus considered to be converged with respect to these variations.

The unsteady Euler calculations for the flat-plate airfoil were then repeated using the cell-centered algorithm to determine the effects of the spatial discretization on the generalized forces. These results and comparisons are presented in Fig. 4. All of the conditions that were used to determine these results were the same as those used to obtain the results of Fig. 3. In contrast with the node-based Euler results, the cell-centered Euler forces are in very good agreement with linear theory, for both plunge and pitch motions, for the entire range of reduced frequency that was considered. Also, the real parts of the

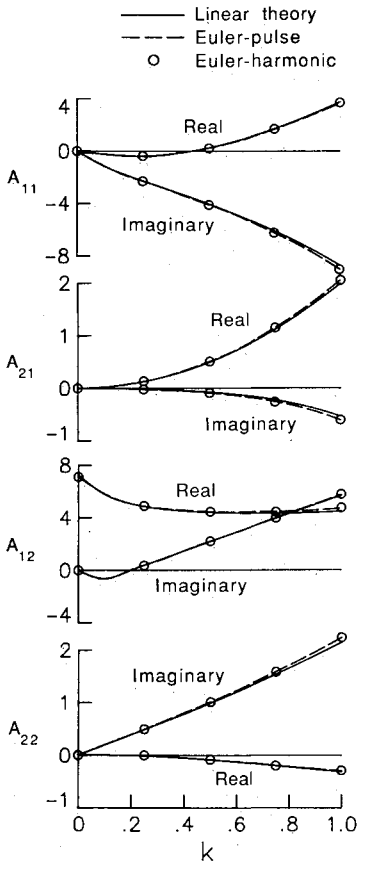

Fig. 4 Comparisons of generalized aerodynamic forces computed using linear theory and the cell-centered Euler algorithm for the flat-plate airfoil at $M_\infty = 0.5$ and $\alpha_0 = 0$ deg.

forces compare slightly better than the imaginary parts. Therefore, because of the improved accuracy provided by the cell-centered discretization, the remainder of the study was conducted using the cell-centered scheme.

Aeroelastic Comparisons

Aeroelastic results for case A were obtained for the flat-plate airfoil using both the state-space and time-marching analyses. The state-space calculations were performed using the generalized aerodynamic forces determined by the Euler pulse analysis and by linear theory. These results are presented in a dynamic pressure root-locus-type format in the complex s plane. The time-marching calculations were performed for three values of dynamic pressure, which bracket the flutter condition, as determined by the state-space analysis. Damping and frequency estimates were determined from the resulting aeroelastic transients using the modal identification technique. These estimates were then compared with values obtained from the state-space calculations to assess the accuracy of the Euler time-marching aeroelastic procedures. A quadratic interpolation of the time-marching dominant damping values was also used to determine the flutter condition, which corresponds to zero damping.

A comparison of nondimensional dynamic pressure root loci for the flat-plate airfoil is presented in Fig. 5. These root loci indicate that the bending- and torsion-mode frequencies approach each other for low values of $\bar{Q}$. The flutter condition is given by the $\sigma = 0$ crossing of the bending root locus, which continues into the unstable right-half plane as the dynamic pressure is increased further. The two sets of root loci agree well with each other, and the values of dynamic pressure at flutter are $\bar{Q}_f = 4.8$ and 4.6, as predicted by the Euler and linear theory analyses, respectively.

Time-marching aeroelastic calculations were performed for $\bar{Q} = 3.0$, 4.0, and 5.0. From these calculations, the generalized displacement of the second coupled mode q_2 as a function of time T is presented in Fig. 6. The two-mode curve fits from the modal identification technique are also given. Note the agreement of the curve fits to the data to within plotting accuracy. These displacement responses show subcritical, near neutrally stable, and unstable aeroelastic behavior corresponding to $\bar{Q} = 3.0$, 4.0, and 5.0, respectively, which is consistent with the state-space results of Fig. 5.

The component modes from the two-mode curve fit of the displacement responses are shown in Fig. 7 for all three cases that were considered. These component modes consist of a dominant mode of larger amplitude corresponding to bending (mode 1) and a second, smaller amplitude, damped mode

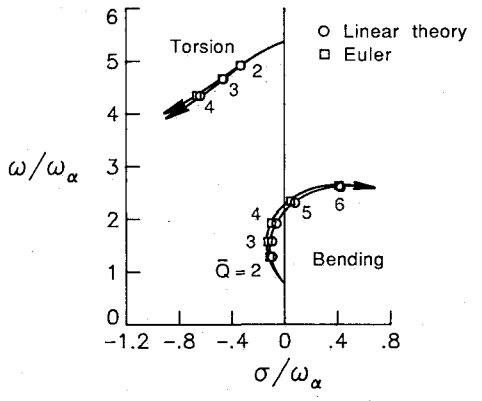

Fig. 5 Comparisons of nondimensional dynamic pressure root loci for the flat-plate airfoil at $M_\infty = 0.5$ and $\alpha_0 = 0$ deg for case A.

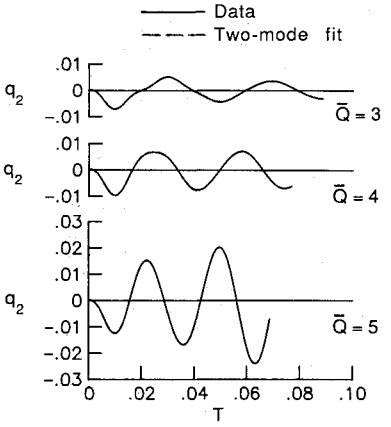

Fig. 6 Effects of nondimensional dynamic pressure on the generalized displacement of the second coupled mode for the flat-plate airfoil at $M_\infty = 0.5$ and $\alpha_0 = 0$ deg for case A.

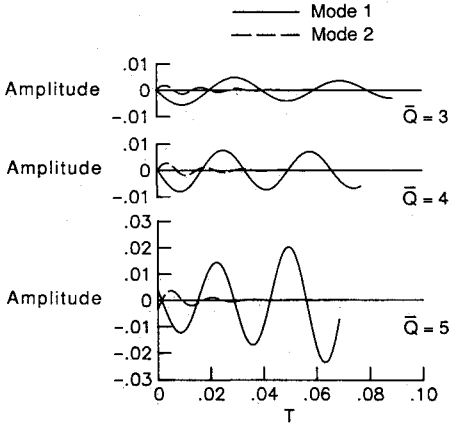

Fig. 7 Effects of nondimensional dynamic pressure on the component modes of the aeroelastic system for the flat-plate airfoil at $M_\infty = 0.5$ and $\alpha_0 = 0$ deg for case A.

Table 1 Comparisons between aeroelastic solutions for the flat-plate airfoil at $M_\infty = 0.5$ and $\alpha_0 = 0$ deg for case A

		Mode 1		Mode 2	
$\bar{Q}$	Method	σ/ω_α	ω/ω_α	σ/ω_α	ω/ω_α
3.0	Linear theory	−0.095	1.578	−0.462	4.658
	Euler state-space	−0.124	1.574	−0.471	4.665
	Euler time-marching	−0.075	1.587	−0.465	4.653
4.0	Linear theory	−0.061	1.913	−0.639	4.341
	Euler state-space	−0.099	1.921	−0.663	4.348
	Euler time-marching	−0.024	1.918	−0.591	4.323
5.0	Linear theory	0.082	2.308	−0.937	3.951
	Euler state-space	0.049	2.339	−0.999	3.955
	Euler time-marching	0.121	2.297	−0.815	4.037

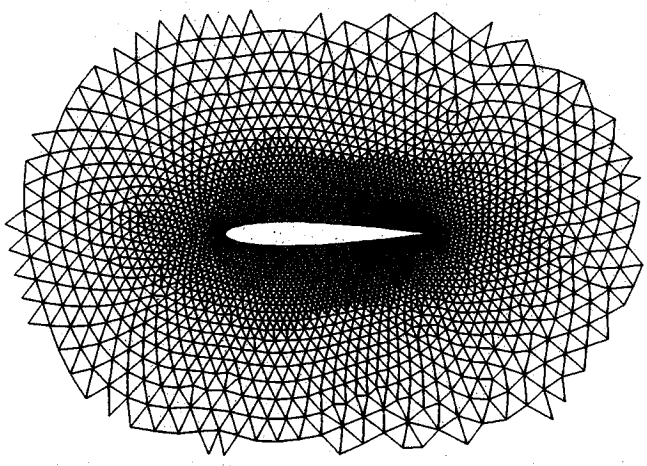

Fig. 8 Partial view of unstructured grid of triangles about the NACA 0012 airfoil.

corresponding to torsion (mode 2). Damping and frequency estimates of the two modes from the curve fits are compared with the state-space model values from the Euler pulse analysis and from linear theory in Table 1. These comparisons indicate that the time-marching values correlate well with the other two sets of results, which tends to verify the Euler time-marching aeroelastic procedures. In general, however, the frequency values agree better than the damping values, as expected. The value of dynamic pressure at flutter from the time-marching analysis was determined to be $\bar{Q}_f = 4.4$, which is within 5% of the linear theory flutter value.

NACA 0012 Airfoil Results

Calculations were performed for the NACA 0012 airfoil to assess the accuracy of the unstructured grid Euler code for transonic applications. The results were obtained using an unstructured grid of triangles, a partial view of which is shown in Fig. 8. The grid has 3300 nodes, 6466 triangles, and extends 20 chord lengths from the airfoil with a circular outer boundary. Also there are 110 points that lie on the surface of the airfoil. Calculations were performed for the airfoil at $M_\infty = 0.8$ and 0 deg angle of attack. Comparisons are made with parallel computations performed using the CFL3D code, run in a two-dimensional mode. The CFL3D code is an Euler/Navier-Stokes code based on cell-centered, upwind-difference discretizations of the governing flow equations based on structured meshes. The CFL3D Euler results that were used in the present study were obtained from Ref. 29, wherein aeroelastic modeling similar to that of the present study was implemented within the code.

Steady Pressure Comparisons

Steady pressure distributions along the upper surface of the NACA 0012 airfoil are presented in Fig. 9. The calculated steady pressures from the Euler code are compared with the experimental steady pressure data of Ref. 30. These pressure distributions indicate that there is a moderately strong shock wave near the midchord of the airfoil. The Euler results compare well with the experimental data in predicting the shock location and strength, as well as the overall pressure levels. This suggests that viscous effects are relatively small for this case.

Generalized Force Comparisons

Generalized aerodynamic forces for the NACA 0012 airfoil are presented in Fig. 10, computed using the unstructured grid Euler pulse analysis, the unstructured grid Euler harmonic analysis, and the CFL3D harmonic analysis. Both sets of harmonic results were obtained at six values of reduced frequency: $k = 0.0, 0.125, 0.25, 0.5, 0.75$, and 1.0. As shown in Fig. 10, the forces from the unstructured grid Euler pulse analysis agree well with the forces from the harmonic analysis.

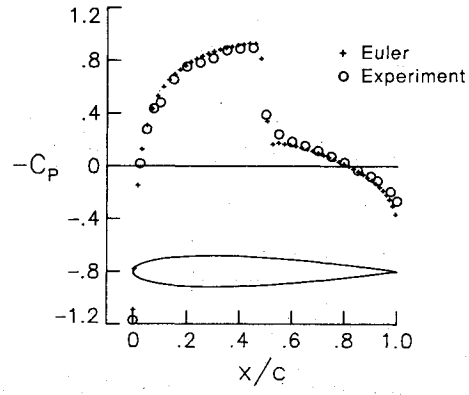

Fig. 9 Comparison of upper surface steady pressure distributions on the NACA 0012 airfoil at $M_\infty = 0.8$ and $\alpha_0 = 0$ deg.

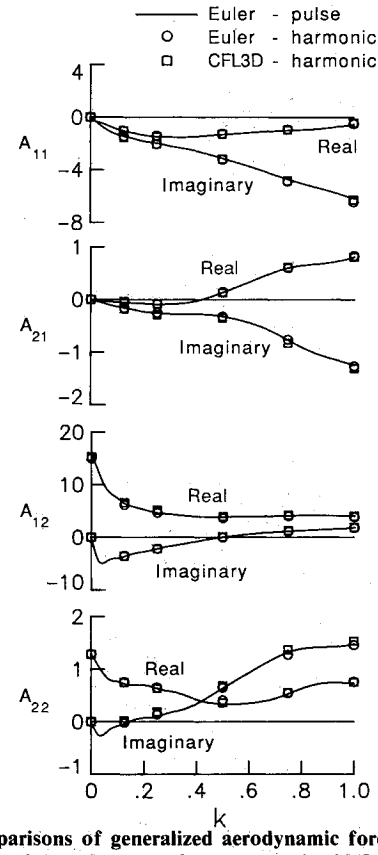

Fig. 10 Comparisons of generalized aerodynamic forces computed using CFL3D and the cell-centered unstructured-grid Euler algorithm for the NACA 0012 airfoil at $M_\infty = 0.8$ and $\alpha_0 = 0$ deg.

The harmonic analysis, however, is considered to be the more accurate of the two sets of calculations because the local linearity assumption in the pulse analysis may be questionable for transonic flow cases. As further shown in Fig. 10, the harmonic forces from the unstructured grid Euler code are in very good agreement with the CFL3D (Euler) harmonic forces, for both plunge and pitch motions, for all values of reduced frequency that were considered.

Aeroelastic Comparisons

Aeroelastic results for case A were obtained for the NACA 0012 airfoil using the time-marching analysis. The calculations were performed for several values of dynamic pressure including $\bar{Q} = 0.2$, 0.3, 0.4, 0.5, 0.6, 0.7, and 0.8 to obtain conditions that bracket the flutter point. Figure 11 shows time responses of the generalized displacement of the second coupled mode for $\bar{Q} = 0.2$, 0.5, and 0.8, which correspond to subcritical, near neutrally stable, and unstable aeroelastic behavior. Also plotted are the corresponding responses computed using CFL3D (Euler).[29] A comparison of these responses indicates that the time-marching aeroelastic results from the unstructured grid Euler code agree well with those from the CFL3D code lending additional confidence in the aeroelastic modeling procedures that were implemented. Shown in Fig. 12 are the two-mode curve fits of the responses from the Euler code again showing excellent approximations to the original data. The component modes from these curve fits are shown in Fig. 13 for the three values of $\bar{Q}$ that were considered in Figs. 11 and 12. Similar to the flat-plate airfoil case of Fig. 7, the NACA 0012 airfoil results of Fig. 13 show that the component modes consist of a dominant mode corresponding to bending (mode 1) and a second higher frequency mode corresponding to torsion (mode 2). Damping and frequency estimates from this analysis are compared with similar values from the CFL3D results in Table 2. These comparisons indicate that the unstructured grid Euler values correlate well with the CFL3D values. Also, the flutter value for $\bar{Q}$, again computed by quadratic interpolation of the damping values, was 0.50 for the Euler code and 0.48 for the CFL3D code. Linear theory at $M_\infty = 0.8$, which of course does not include transonic effects, predicts a much higher value of 1.89.

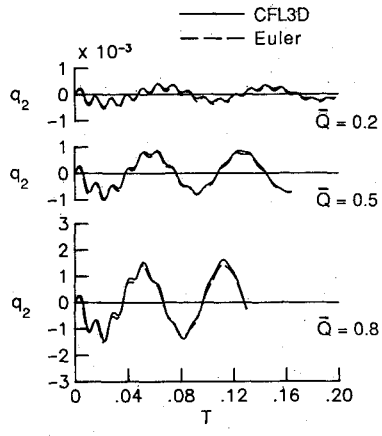

Fig. 11 Comparisons of generalized displacements computed using CFL3D and the unstructured-grid Euler code for the NACA 0012 airfoil at $M_\infty = 0.8$ and $\alpha_0 = 0$ deg for case A.

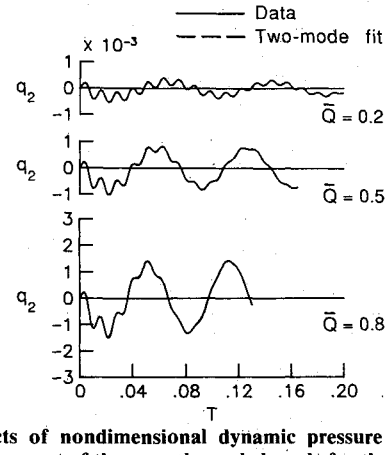

Fig. 12 Effects of nondimensional dynamic pressure on the generalized displacement of the second coupled mode for the NACA 0012 airfoil at $M_\infty = 0.8$ and $\alpha_0 = 0$ deg for case A.

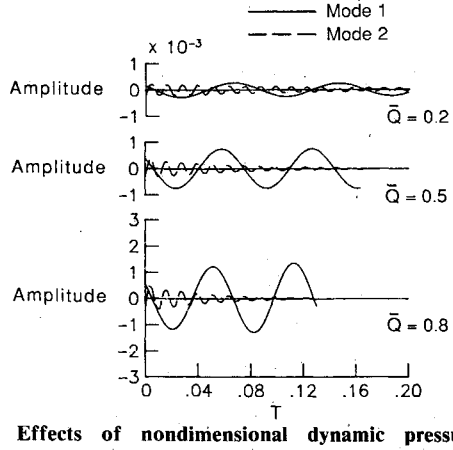

Fig. 13 Effects of nondimensional dynamic pressure on the component modes of the aeroelastic system for the NACA 0012 airfoil at $M_\infty = 0.8$ and $\alpha_0 = 0$ deg for case A.

Table 2 Comparisons between aeroelastic solutions for the NACA 0012 airfoil at $M_\infty = 0.8$ and $\alpha_0 = 0$ deg for case A

		Mode 1		Mode 2	
$\bar{Q}$	Method	σ/ω_α	ω/ω_α	σ/ω_α	ω/ω_α
0.2	CFL3D time-marching	−0.011	0.794	−0.091	5.363
	Euler time-marching	−0.011	0.790	−0.068	5.353
0.5	CFL3D time-marching	0.004	0.914	−0.185	5.347
	Euler time-marching	0.000	0.913	−0.148	5.349
0.8	CFL3D time-marching	0.026	1.027	−0.173	5.270
	Euler time-marching	0.017	1.022	−0.223	5.317

Concluding Remarks

Modifications to a two-dimensional, unsteady Euler code based on unstructured grid methods for the aeroelastic analysis of airfoils were described. This involved the addition of the structural equations of motion for their simultaneous time integration with the governing flow equations. The flow solver of the Euler code involves a multistage, Runge-Kutta, time-stepping scheme, which uses a finite-volume spatial discretization. Results for node-based and cell-centered types of discretizations of the Euler equations were presented. The code also includes a dynamic mesh algorithm that is capable of treating general aeroelastic motions. Results were presented for the flat-plate airfoil and the NACA 0012 airfoil to demonstrate applications of the Euler code to generalized aerodynamic force computation and aeroelastic analysis. Detailed comparisons of results from the two-dimensional Euler code, the CFL3D Euler/Navier-Stokes code, and linear theory were made. For the flat-plate airfoil, comparisons between generalized forces obtained using the Euler code and linear theory showed that a cell-centered Euler scheme was superior in accuracy to a node-based scheme. For the NACA 0012 airfoil at transonic flow conditions, comparisons with generalized forces obtained from CFL3D (Euler) showed that the cell-centered unstructured grid Euler code is also accurate for transonic unsteady cases.

Aeroelastic results were presented for two-degree-of-freedom airfoils to demonstrate application of the Euler code for such analyses. Results from both time-marching and state-space aeroelastic analyses using the Euler code were compared with linear theory results for the flat-plate airfoil case. Damping and frequency characteristics of the aeroelastic modes were in good agreement, and the dynamic pressure at flutter agreed to within 5%. For the NACA 0012 airfoil, the transonic, time-marching, aeroelastic results compared well with similar results from CFL3D and the flutter dynamic pressures agreed to within 4%.

Acknowledgments

The work constitutes a part of the first author's M.S. Thesis at Purdue University and was supported by the NASA Langley Graduate Aeronautics Program under Grant NAG-1-372. Also, the authors would like to thank Paresh Parikh of Vigyan Research Associates, Hampton, Virginia, and Rainald Lohner of George Washington University, Washington, DC, for providing the grid generation program that was used to generate the grid for the NACA 0012 airfoil in the present study.

References

[1]Edwards, J. W., and Thomas, J. L., "Computational Methods for Unsteady Transonic Flows," AIAA Paper 87-0107, Jan. 1987.

[2]Borland, C. J., and Rizzetta, D. P., "Nonlinear Transonic Flutter Analysis," *AIAA Journal,* Vol. 20, No. 11, 1982, pp. 1606–1615.

[3]Batina, J. T., Seidel, D. A., Bland, S. R., and Bennett, R. M., "Unsteady Transonic Flow Calculations for Realistic Aircraft Configurations," AIAA Paper 87-0850, April 1987.

[4]Isogai, K., and Suetsuga, K., "Numerical Simulation of Transonic Flutter of a Supercritical Wing," National Aerospace Lab., Tokyo, Japan, Rept. TR-276T, Aug. 1982.

[5]Ide, H., and Shankar, V. J., "Unsteady Full Potential Aeroelastic Computations for Flexible Configurations," AIAA Paper 87-1238, June 1987.

[6]Bendiksen, O. O., and Kousen, K. A., "Transonic Flutter Analysis Using the Euler Equations," AIAA Paper 87-0911, April 1987.

[7]Kousen, K. A., and Bendiksen, O. O., "Nonlinear Aspects of the Transonic Aeroelastic Stability Problem," AIAA Paper 88-2306, April 1988.

[8]Wu, J., Kaza, K. R. V., and Sankar, L. N., "A Technique for the Prediction of Airfoil Flutter Characteristics in Separated Flow," AIAA Paper 87-0910, April 1987.

[9]Reddy, T. S. R., Srivastava, R., and Kaza, K. R. V., "The Effects of Rotational Flow, Viscosity, Thickness, and Shape on Transonic Flutter Dip Phenomena," AIAA Paper 88-2348, April 1988.

[10]Guruswamy, G. P., "Time-Accurate Unsteady Aerodynamic and Aeroelastic Calculations of Wings Using Euler Equations," AIAA Paper 88-2281, April 1988.

[11]Mavriplis, D., and Jameson, A., "Multigrid Solution of the Two-Dimensional Euler Equations on Unstructured Triangular Meshes," AIAA Paper 87-0353, Jan. 1987.

[12]Morgan, K., Peraire, J., Thareja, R. R., and Stewart, J. R., "An Adaptive Finite Element Scheme for the Euler and Navier-Stokes Equations," AIAA Paper 87-1172, June 1987.

[13]Jameson, A., Baker, T. J., and Weatherill, N. P., "Calculation of Inviscid Transonic Flow Over a Complete Aircraft," AIAA Paper 86-0103, Jan. 1986.

[14]Peraire, J., Peiro, J., Formaggia, L., and Morgan, K., "Finite Element Euler Computations in Three Dimensions," AIAA Paper 88-0032, Jan. 1988.

[15]Lohner, R., and Morgan, K., "Improved Adaptive Refinement Strategies for Finite Element Aerodynamic Computations," AIAA Paper 86-0499, Jan. 1986.

[16]Peraire, J., Morgan, K., Peiro, J., and Zienkiewicz, O. C., "An Adaptive Finite Element Method for High Speed Flow," AIAA Paper 87-0558, Jan. 1987.

[17]Batina, J. T., "Unsteady Euler Airfoil Solutions Using Unstructured Dynamic Meshes," AIAA Paper 89-0115, Jan. 1989.

[18]Batina, J. T., "Unsteady Euler Algorithm with Unstructured Dynamic Mesh for Complex-Aircraft Aeroelastic Analysis," AIAA Paper 89-1189, April 1989.

[19]Anderson, W. K., Thomas, J. L., and Rumsey, C. L., "Extension and Applications of Flux-Vector Splitting to Unsteady Calculations on Dynamic Meshes," AIAA Paper 87-1152, June 1987.

[20]Bland, S. R., "Development of Low-Frequency Kernel-Function Aerodynamics for Comparison with Time-Dependent Finite-Difference Method," NASA TM 83283, May 1982.

[21]Seidel, D. A., Bennett, R. M., and Whitlow, W., Jr., "An Exploratory Study of Finite Difference Grids for Transonic Unsteady Aerodynamics," AIAA Paper 83-0503, Jan. 1983.

[22]Seidel, D. A., Bennett, R. M., and Ricketts, R. H., "Some Recent Applications of XTRAN3S," AIAA Paper 83-1811, July 1983.

[23]Edwards, J. W., Bennett, R. M., Whitlow, W., Jr., and Seidel, D. A., "Time-Marching Transonic Flutter Solutions Including Angle-of-Attack Effects," *Journal of Aircraft,* Vol. 20, No. 11, 1984, pp. 899–906.

[24]Edwards, J. W., Bennett, R. M., Whitlow, W., Jr., and Seidel, D. A., "Time-Marching Transonic Flutter Solutions Including Angle-of-Attack Effects," AIAA Paper 82-3685, May 1982.

[25]Bennett, R. M., and Desmarais, R. N., "Curve Fitting of Aeroelastic Transient Response Data with Exponential Functions," *Flutter Testing Techniques,* NASA SP-415, May 1975, pp. 43–58.

[26]Batina, J. T., and Yang, T. Y., "Application of Transonic Codes to Aeroelastic Modeling of Airfoils Including Active Controls," *Journal of Aircraft,* Vol. 21, No. 8, 1984, pp. 623–630.

[27]Batina, J. T., and Yang, T. Y., "Transonic Calculation of Airfoils Stability and Response with Active Controls," AIAA Paper 84-0873, May 1984.

[28]Isogai, K., "Numerical Study of Transonic Flutter of a Two-Dimensional Airfoil," National Aerospace Laboratory, Tokyo, Japan, TR-617T, July 1980.

[29]Robinson, B. A., "Time-Marching Aeroelastic Analysis of Wings Using the Euler Equations with a Deforming Mesh," M.S. Thesis, Purdue Univ., West Lafayette, IN, May 1989.

[30]McDevitt, J. B., and Okuno, A. F., "Static and Dynamic Pressure Measurements on a NACA 0012 Airfoil in the Ames High Reynolds Number Facility," NASA TP-2485, June 1985.